JOURNAL OF MATERIALS SCIENCE 35 (2000) 4165–4176

Effect of barrier layer thickness and composition on fracture toughness of layered zirconia/alumina composites

H. TOMASZEWSKI, H. WĘGLARZ, M. BONIECKI
Institute of Electronic Materials Technology, 01-919 Warsaw, Poland
E-mail: tomasz_h@sp.itme.edu.pl

W. M. REĆKO
Institute of Glass and Ceramics, 02-676 Warsaw, Poland

Composites of yttria or ceria-partially-stabilized zirconia with layers of either alumina or a mixture of 50% by volume of alumina and zirconia were fabricated by sequential centrifuging of powder suspensions. This method allowed formation of layers with thickness of 10 to 70 μm. In both cases (Y-ZrO_2 and Ce-ZrO_2 matrices), a significant increase in fracture toughness, work of fracture and bending strength was observed only for composites with barrier layers made of a pure alumina. A crack deflection in alumina layer was found to be the main mechanism responsible for an increase in mechanical properties. For confirmation this thesis, no increase in the transformation zone width was observed. As it was shown, crack deflection angle was dependent on alumina layer thickness. Higher deflection angles for a thicker alumina layers were found. Explanation of this phenomenon was given by determination of residual stress distribution in barrier layers made by piezospectroscopy. A correlation between the crack deflection angle and the difference of stress between the layer boundary and the centre of the layer was noticed. The residual stresses observed are a result of thermal expansion mismatch between alumina and zirconia and thermal anisotropy of alumina. Shrinkage mismatch, especially in the case of Ce-ZrO_2 and Al_2O_3, as a third source of stress is suggested.

1. Introduction

Since the discovery of transformation toughening in ZrO_2 in 1975 [1], a variety of toughened ZrO_2-based materials (Mg-PSZ, Y-TZP, Ce-TZP) with high toughness have been developed. Up to now, the mechanism of transformation toughening has been well known [2–4] and some models have been presented [2, 5, 6] to account for the considerable toughness enhancement that is observed in ceramic systems containing tetragonal ZrO_2. The models predict that the increase in toughness is linked with the size and shape of the transformation zone. A new way of optimising the transformation zone surrounding cracks in Ce-TZP was developed by Marshall *et al.* in 1991 [7, 8]. By introducing Al_2O_3 or Al_2O_3/ZrO_2 layers into Ce-TZP, they observed an increased toughening due to spreading of the transformation zone.

The aim of this work was to investigate laminar microcomposites containing layers of Y-ZrO_2 or Ce-ZrO_2 and either Al_2O_3 or a mixture of Al_2O_3 and ZrO_2 fabricated by sequential centrifugation of aqueous particle suspensions. In our work spreading of the transformation zone has not been observed, but similar increases in toughness have been obtained. The toughness has been related to crack deflection in the barrier layers the extent of that was dependent on layer thickness and composition. This crack deflection mechanism has been known previously to achieve toughening in multilayered ceramic composites containing weak layers or interfaces [9–11]. In our study of strongly bonded interfaces, the degree of crack deflection was linked with the distribution of residual compressive stresses.

To understand the crack deflection phenomena He and Hutchinson [12] considered the effect of an interface between two dissimilar materials. Their analysis defines the conditions under which the crack will deflect into the interface rather than extend into the adjacent materials. It includes the effect of the elastic mismatch between the two materials. Later, He and Evans [13] modified the analysis to include the effects of residual stress. Recently, a phenomenon of the formation of an edge crack along the centreline of the layer under compression, directly related as a new crack deflection mechanism, i.e., the bifurcation of a crack, was reported by Ho *et al.* [14] and Oechner *et al.* [15]. This phenomenon has proved to be very helpful in understanding of the results of presented work.

TABLE I Ceramic powders used for preparing of microlayered composites

Powder type	Powder chemical composition	Producer	Grain size, μm	Application
TZ-12Ce	ZrO_2 + 12 mol% CeO_2	Tosoh, Japan	0.3	Matrix layer
	ZrO_2 + 3.4 mol% Y_2O_3	Unitec Ceramics, Great Britain	0.6	Matrix layer
AKP 53	Al_2O_3	Sumitomo, Japan	0.29	Barrier layer

TABLE II Shrinkage of the matrix and barrier layer materials in sintering temperature

Material	Linear shrinkage after sintering in 1600°C, %
Y-ZrO_2	19.04
Ce-ZrO_2	21.39
Al_2O_3	16.27
Mixture of Al_2O_3 and Y-ZrO_2	18.47
Mixture of Al_2O_3 and Ce-ZrO_2	18.60

2. Experimental procedure

Composites of Y-ZrO_2 or Ce-ZrO_2 with alumina layers with thickness of 10 to 70 μm were fabricated by the sequential centrifuging (Model Z382, Hermle) of powder suspensions (Table I). Aqueous slurries containing 5 to 10 wt% of subsequent powders were prepared by ultrasonicating the powders in deionized water at pH 4. Cast samples were dried, additionally isostatically pressed at 120 MPa and then sintered at 1600°C. To minimise the shrinkage mismatch of Y-ZrO_2, Ce-ZrO_2 and Al_2O_3, in some layered composites the mixed composition of 50 vol% alumina and zirconia was used instead of a pure Al_2O_3 (Table II). The samples after sintering were cut and ground to the dimensions of $45 \times 4 \times 4$ mm or $45 \times 4 \times 1.5$ mm and one surface perpendicular to the layers was polished. A sharp notch in the centre of the beams was prepared with two diamond saws: 0.200 and 0.025 mm.

The bending strength of the composites was determined on square bars with the dimensions $45 \times 4 \times 4$ mm perpendicular to the layers, in three-point bending tests using a universal testing machine (Model 1446, Zwick) with 1 mm/min loading speed and 40 mm bearing distance.

For measurement of Young's modulus the beams were trimmed to the height of 1 mm and then the compliance of the samples was recorded during loading tests with 0.1 mm/min loading speed and 40 mm bearing distance. The values of Young's modulus were determined using the relationship given by Fett and Munz [16], which is stated in Equation 3 below.

The critical stress intensity factor, K_{Ic}, was measured by using Evans's [17] method, on notched beams ($45 \times 4 \times 4$ mm, notch ~1 mm) perpendicular to the layers in three-point bending test. The bearing spacing was 40 mm and the rate of loading 1 mm/min.

The controlled crack growth tests were performed in three-point bending with 1 μm/min loading speed and 40 mm bearing distance using the same testing machine. The crack was initiated and slowly grown by repeated loading and unloading. The procedure results in an increase of crack length by one-step less than 100 μm. The path of the crack during the fracture of layered composite was registered by SEM (using microscope model OPTON DSM 950). All experiments were done at room temperature in a normal air environment. In several samples the crack growth tests were done without unloading. The time dependent displacement, d, of the sample was measured and recorded together with values of force, P. According to Fett and Munz [16], the total compliance, C, indicated by Equation 1

$$C = \frac{d}{P} \tag{1}$$

consists of the compliance of the measuring system, C_u, the compliance of the uncracked bar, C_0, and the portion ΔC caused by the crack.

$$C = C_u + C_0 + \Delta C \tag{2}$$

with

$$C_0 = \frac{L^2}{w^2 B E}\left[\frac{L}{4w} + (1+\nu)\frac{w}{2L}\right] \tag{3}$$

where E is Young's modulus, ν is Poisson's ratio, w is the specimen thickness, B is the specimen width and L is the bearing distance. The compliance part due to the crack could be obtained from ref. [16] as

$$\Delta C = 4.5\frac{L^2}{w^2 E B}\left(\frac{a}{1-a}\right)^2 \sum_{i=0}^{5}\sum_{j=0}^{3} B_{ij} a^i \left(\frac{w}{L}\right)^j \tag{4}$$

with $a = c/w$, where c is the length of the crack and B_{ij} are the coefficients given by Fett and Munz [18].

The stress intensity factor K_I values have been determined from the relation (5)

$$K_I = 1.5\frac{PL}{w^2 B} Y c^{\frac{1}{2}} \tag{5}$$

using the geometric function Y, stated below in Equation 6, with the coefficients A_{ij} given by Fett and Munz [18].

$$Y = \frac{\sqrt{\Pi}}{(1-a)^{\frac{3}{2}}}\left[0.3738a + (1-a)\sum_{i,j=0}^{4} A_{ij} a^i \left(\frac{w}{L}\right)^j\right] \tag{6}$$

The crack growth rate $v = \mathrm{d}c/\mathrm{d}t$ controlled by the stress intensity factor, K_I, was calculated from the time dependent crack length, c. Assuming a power-law relation between v and K_I

$$v = \frac{\mathrm{d}c}{\mathrm{d}t} = A K_I^n \tag{7}$$

the parameters A (or $\log A$) and n could be obtained.

Given that the area under the recorded load-deflection curve of the specimen is the sum of the work used for creating of two new surfaces and the elastic strain energy of the system and sample studied, the work-of-fracture, γ_F, was determined:

$$\gamma_F = \frac{U}{2A} \tag{8}$$

where U is the total deformation work of a specimen up to fracture and A is the area of fractured cross-section of the specimen.

The spatial distribution of residual stresses within the alumina and a mixture of alumina and zirconia layer of the composites were measured using the piezospectroscopic technique. This method is based on the photo-stimulated fluorescence from trace Cr^{+3} ions in alumina. The frequency shift $\Delta\nu$ of the two lines in the R-doublet is a measure of the elastic strain within the volume of material excited by the laser, following tensorial relation [19]:

$$\Delta\nu = \Pi_{ij}\sigma_{ij} \tag{9}$$

where: Π_{ij} are the piezospectroscopic coefficients and σ_{ij} are the stress components.

The piezospectroscopic measurements were made using an optical microscope with an attached spectrometer (Model DILOR X4800). An argon ion laser operating at a wavelength of 514.5 nm was used as the excitation source. In each experiment an area of interest in the sample was first selected using the microscope then a laser beam was focused on a spot in that area. In this way, the pure alumina or mixture layers of composites were scanned by 5 to 10 μm steps. The intensities of the stimulated R_1 and R_2 fluorescence lines were collected by scanning the spectrometer gratings using steps of 0.2–0.4 wave numbers and integrating them over 0.5 s intervals. The collected data was subsequently analysed with curve-fitting algorithms (double Lorenz function). The line position was identified by simultaneously fitting the R_1 and R_2 peaks using NiceFit software package. By using an objective lens of 100× magnifying power, a minimum spot size of ~3 μm diameter could be achieved. It is known that both R_1 and R_2 lines shift to a smaller wave number with increasing temperature, so a consistent calibration for a ruby was performed. Monitoring an external reproducible spectral line of a neon discharge lamp compensated for instrumental fluctuations. For determining the stresses in alumina the R_1 line and piezospectroscopic coefficients found by He and Clarke [19] have been used.

The width of the transformation zone over the wake of the crack was determined by Nomarski and optical interference using metallographic microscope (Model MeF2, Reichert).

3. Results

3.1. Layered Y-ZrO_2/Al_2O_3 composites

In general, since the thermal expansion coefficients of the two materials of layered composites are different, residual strain can develop during cooling from fabrication temperature. In the layer with lower α ($\alpha_{Al2O3} = 9\times10^{-6}\,^{\circ}C^{-1}$) the biaxial compressive stress is expected and similarly, the biaxial tensile stress in the layer with higher α ($\alpha_{ZrO2} = 12\times10^{-6}\,^{\circ}C^{-1}$). Such a stress distribution (Fig. 1) indicates that the expected tensile stress in the zirconia layer should cause opening of the crack in the notched beam during bending. On the contrary, the compressive stress in alumina layer will prevent the opening of the crack. This expectation was confirmed by the tests of crack initiation in the notched beams of composite studied. It would appear that for the same layer thickness and bearing distance, 25% higher force had to be used to initiate the crack in a sample where the notch ended at the beginning of the alumina layer in comparison to the sample where it ended in zirconia layer. The character of the crack path during fracture was also different in these two samples. In the case of the first sample (notch ended at the beginning of alumina layer), the crack was deflected at the beginning of its path through the alumina layer (see Fig. 2). In the case of the second sample, the initiated crack propagated through zirconia layer perpendicularly to the layers.

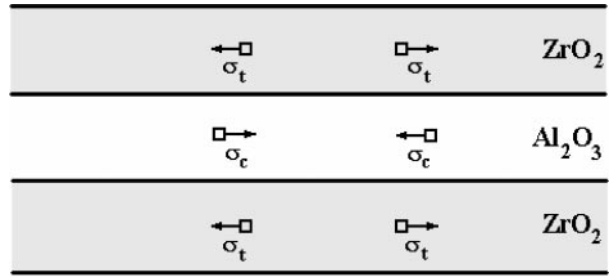

Figure 1 Expected stress distribution in layered zirconia-alumina composites: σ_t - tensile stresses, σ_c - compressive stresses.

Further observations of the controlled crack growth showed that deflection of crack takes place only in the alumina layer. In the zirconia layer the crack deflects back to its original direction. At the beginning of the crack, the deflection process in alumina layers is more complicated than it is shown in Figs 1 and 2. The crack not only deflects but also branches (see Fig. 3) which distinctly enhances the length of the crack's path and energy release during the fracture through the alumina layer. It would appear that the degree of the crack deflection is dependent on the thickness of the alumina layer. The values of the crack deflection angle in terms of layer thickness are listed in Table III. As can be seen, this angle increases with layer thickness. For example, at 60 μm thick alumina layer the crack deflects at 90° (see Fig. 4). In layers with a thickness of 10 μm and lower, deflection does not take place (Fig. 5). The crack behaviour described was observed not only on the cut surfaces but also in the bulk of the material studied.

Generally, the deflection process is linked with the effect of the thermal and elastic mismatch between two materials of the layered composite [12]. A distinct elastic mismatch is present between Al_2O_3 and ZrO_2 ($E_{Al2O3} = 400$ GPa, $E_{ZrO2} = 200$ GPa), but residual stresses found in barrier layers seem to be the most important parameter responsible for the crack deflection.

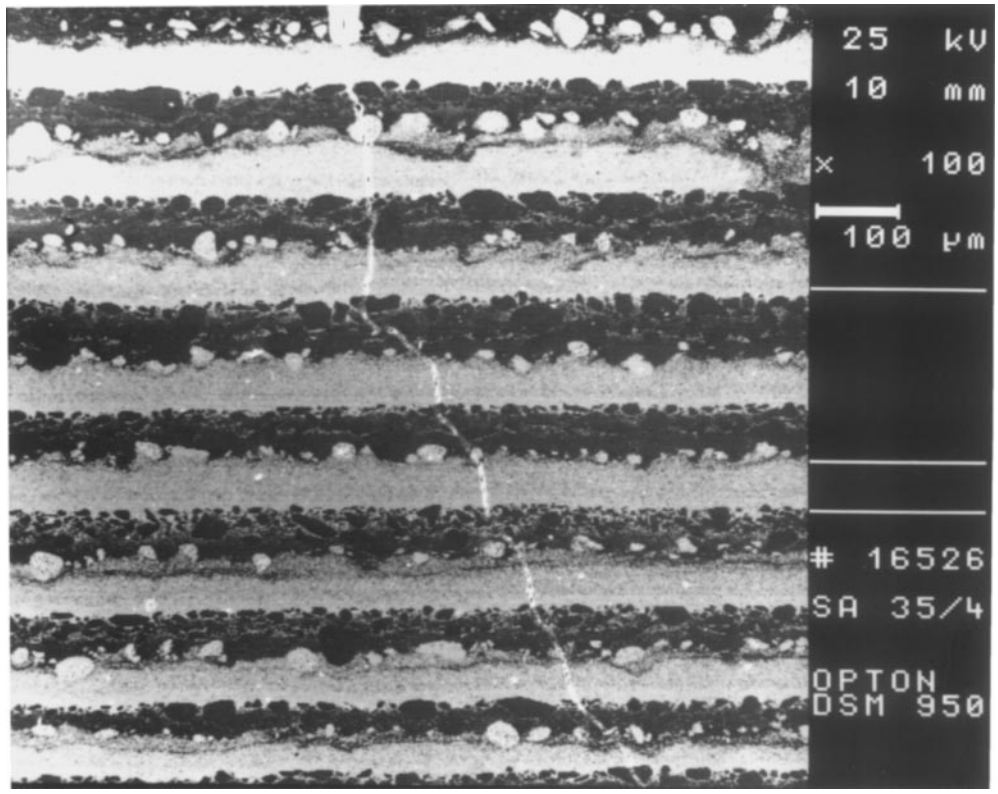

(a)

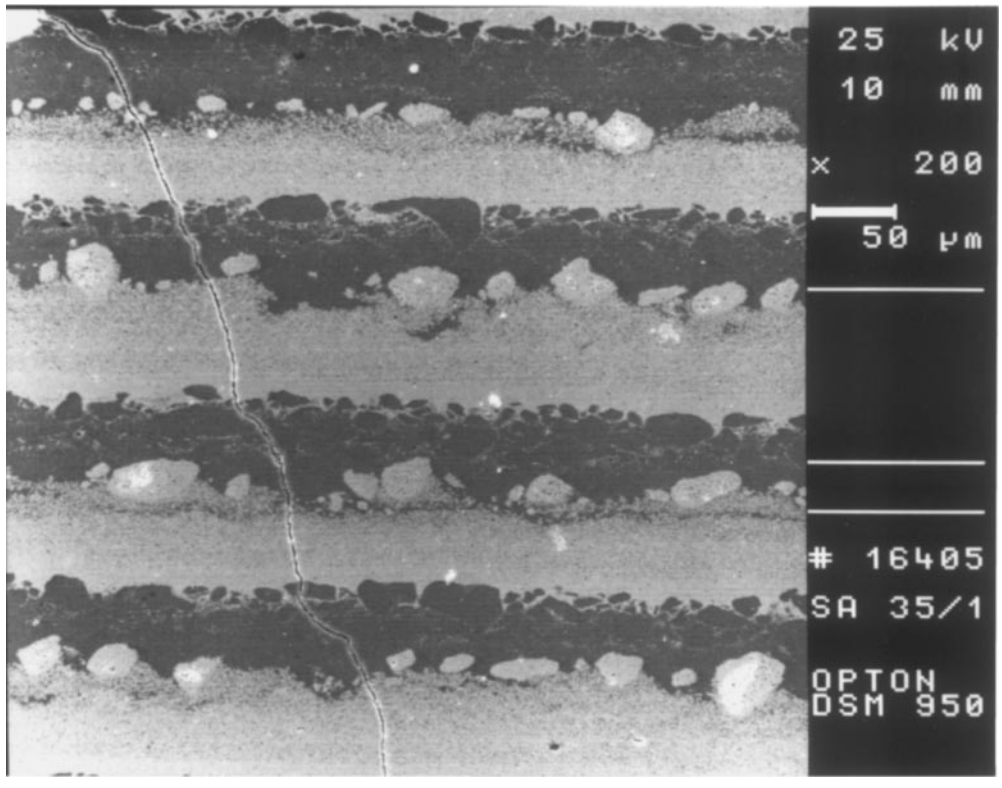

(b)

Figure 2 Character of crack path in layered Y-ZrO_2/Al_2O_3 composite dependent on the type of layer where notch has been made: a) the end of the notch in the zirconia layer - *the crack propagates perpendicularly to the layer*, b) the end of the notch in the alumina layer - *the crack immediately deflects*.

As can be seen from Fig. 6, the compressive stress in alumina layers calculated from the frequency shift of the R_1 line is not only a function of barrier layer thickness but also a position across the layer. The maximum of the compressive stress equalled 280 MPa is observed at the interfaces and it is independent on alumina layer thickness. Minimum stress is achieved in the centre of the layer. The minimum stress was found to be dependent on the thickness of the alumina layer. In the case of the 60 μm thick barrier layer the minimum equals 88.3 MPa. This value is exactly equal to the residual stresses measured in an alumina pellet

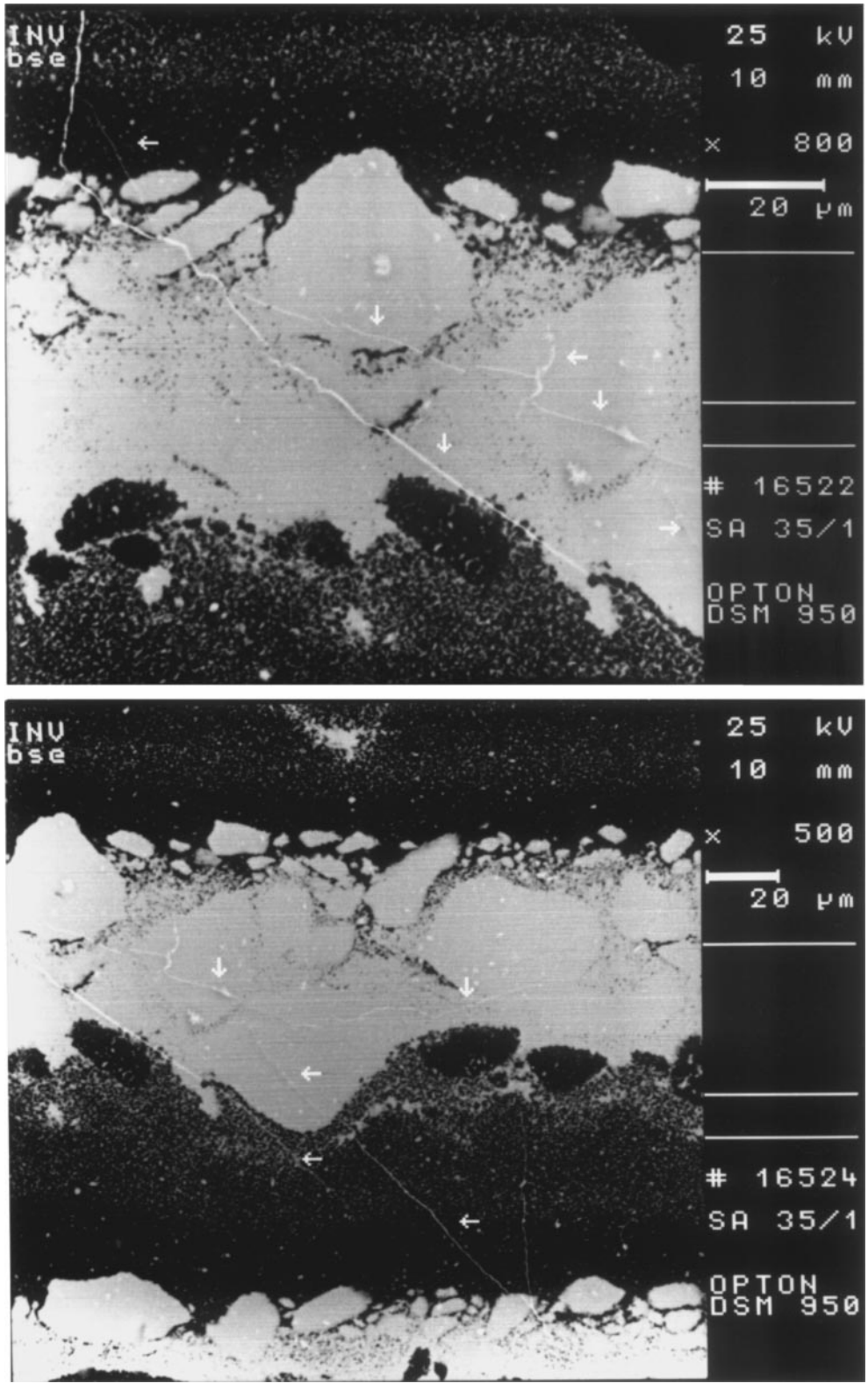

Figure 3 The crack path in the alumina layer of Y-ZrO_2/Al_2O_3 composite at the crack front (inverted image).

TABLE III Crack deflection angle and difference of compressive stress in alumina layer of Y-ZrO_2/Al_2O_3 composite as a function of layer thickness

Thickness of alumina layer, μm	Crack deflection angle, $^\circ$	Difference of compressive stress, MPa
10	0	13.2
25	22 ± 5	50.8
40	62 ± 8	158.1
60	90	188.4

prepared from the same type of alumina powder and sintered at the same temperature but caused by thermal anisotropy of the alumina.

The Table III shows the difference in compressive stress between the layer boundary and the centre of the layer correlates with the angle of crack deflection. Good correspondence observed indicates that the magnitude of the stress difference can be regarded as an important factor responsible for the degree of crack deflection and a further contribution to the crack deflection mechanism

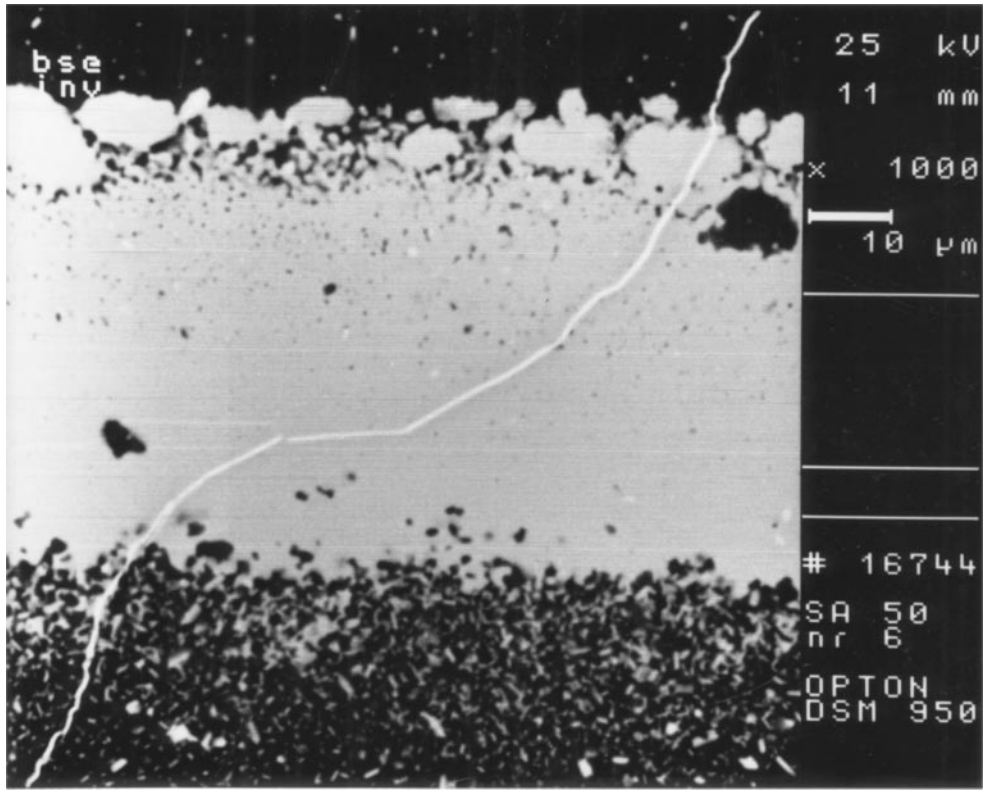

Figure 4 The crack path in the 55 μm thick alumina layer of Y-ZrO_2/Al_2O_3 composite (inverted image).

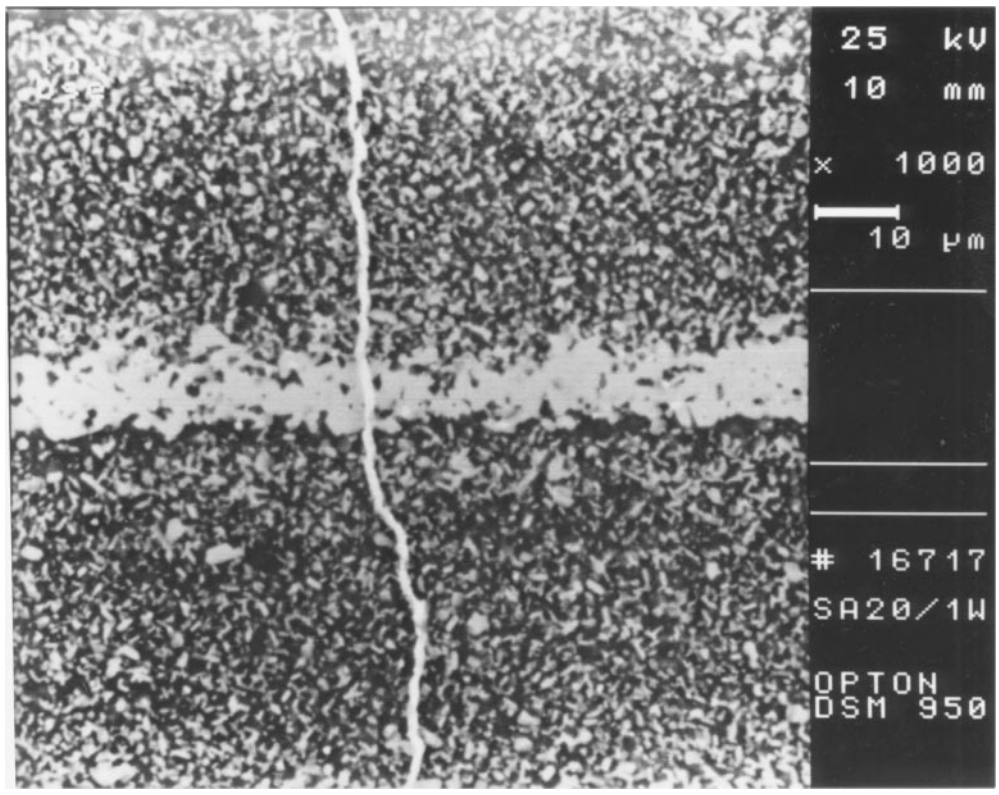

Figure 5 The crack path in the 8.2 μm thick alumina layer of Y-ZrO_2/Al_2O_3 composite (inverted image).

in enhancing the toughness observed in layered composites.

The importance of the role of compressive stress differences in the process of crack deflection confirms the crack path observed in composites with barrier layers made of an oxide mixture instead of a pure Al_2O_3 and prepared to minimise the larger shrinkage of Y-ZrO_2 (see Table II). As can be seen from Fig. 7 the crack propagates through the barrier layer without deflection, independently of the layer thickness. The compressive stress in this case is distinctly higher than in the layer made of pure alumina but independent of position across the layer (Fig. 8). The compressive stress difference is zero.

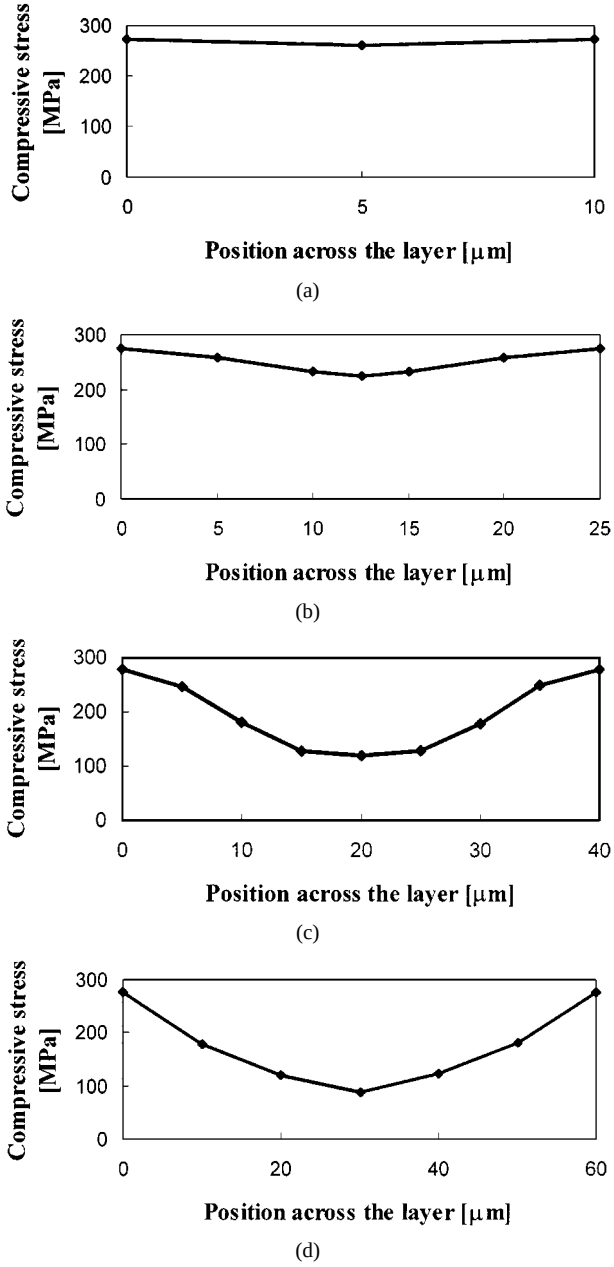

Figure 6 Distribution of compressive stress in the alumina layer with thickness of: a) 10 μm, b) 25 μm, c) 40 μm and d) 60 μm, of Y-ZrO_2/Al_2O_3 composite as a function of position across the layer.

Crack deflection in alumina layers dependent on layer thickness results in an increase in toughness of Y-ZrO_2/Al_2O_3 composites. Table IV shows bending strength, critical stress intensity factor and work-of-fracture increase with the alumina barrier layer thickness and it reaches the maximum for the thick layers. In the case of the thinnest layers, where crack deflection is not observed the above mentioned properties do not differ from the values represented by composites with barrier layers made from a mixture or the same Y-TZP matrix. Similar changes are observed in the crack growth rate v and character of v-K_I curve. The crack growth rate for composites with 60 μm thick alumina layers, described by parameter n and log A, is much lower in comparison to the same of composites with 10 μm thick alumina layers, where crack deflection was not found. A plot of v-K_I obtained for composite with 60 μm thick alumina layers is shown in Fig. 9. Points on this plot where $v \to 0$ can be interpreted as a crack arrest in barrier layers or as an effect of crack propagation in a direction parallel to the layers. For comparison, Fig. 10 shows a plot of v-K_I for composite with barrier layers made of a mixture. As can be seen either the character of the curve or the values of parameters n and log A in this case are similar to those of the matrix.

The determination of the transformation zone width is confirmation of the thesis that crack deflection is the only mechanism responsible for the observed increase in the toughness of Y-ZrO_2/Al_2O_3 composites. The zone width of the Y-TZP matrix equals 3–5 μm, but the height of the uplift observed in optical interference is about 0.8 μm. The same measurements made for Y-ZrO_2/Al_2O_3 composites showed no increase in width and height, independent of the layer thickness and composition.

3.2. Layered Ce-ZrO_2/Al_2O_3 composites

As it shown in Table II, the sintering shrinkage mismatch between Ce-ZrO_2 and Al_2O_3 is higher than 5%. Preparing the oxide mixture reduces this mismatch only to about 2.4%. The test of controlled crack growth in Ce-ZrO_2/Al_2O_3 showed similar dependence on barrier layer composition as was found in Y-ZrO_2/Al_2O_3 composites. In the case of barrier layers made of a mixture the crack does not undergo deflection (Fig. 11) independently of layer thickness and layer thickness does not affect the mechanical properties and parameters n and log A of composites in comparison to the same properties of Ce-ZrO_2 matrix (Table V). Distinct changes in properties of Ce-ZrO_2/Al_2O_3 composites have been found when the barrier layers made of a mixture were exchanged for pure alumina. The result was an 80%

TABLE IV Properties of Y-ZrO_2/Al_2O_3 composite as a function of barrier layer thickness and composition

Barrier layer composition	Alumina				Mixture of Al_2O_3 and Y-ZrO_2	Matrix of Y-ZrO_2
Layer thickness, μm	10	25	40	60	45	-
Young's modulus, GPa	286.4 ± 5.7	286.4 ± 5.7	286.4 ± 5.7	286.4 ± 5.7	227.3 ± 5.0	195.4 ± 1.0
Bending strength, MPa	425 ± 63	566 ± 100	712 ± 136	808 ± 40	644 ± 141	417 ± 108
K_{Ic}, MPa $m^{1/2}$	7.20 ± 0.15	8.42 ± 0.55	9.99 ± 0.76	10.00 ± 0.33	7.11 ± 0.41	7.32 ± 0.20
Work-of-fracture, J/m^2	39.8 ± 8.30	47.06 ± 3.25	52.83 ± 5.80	58.88 ± 5.30	38.15 ± 3.50	37.38 ± 5.46
Parameter n	49.5 ± 15.1	15.7 ± 2.5	3.7 ± 0.7	3.7 ± 1.3	43.9 ± 6.0	53.1 ± 7.0
Parameter log A	-34.5 ± 11.4	-16.6 ± 2.1	-8.7 ± 0.5	-8.0 ± 1.1	-36.5 ± 5.2	-38.7 ± 3.6

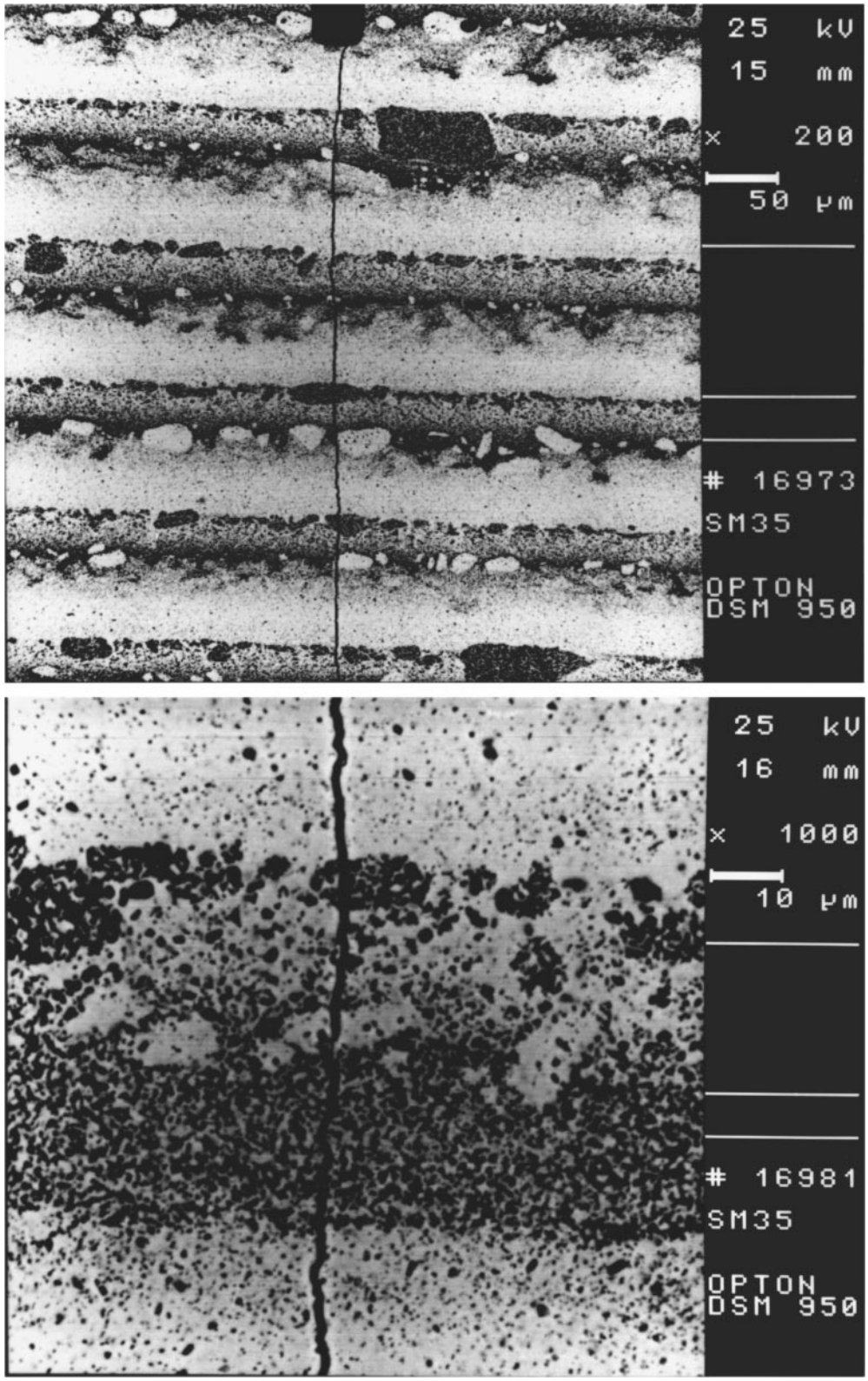

Figure 7 The crack path during fracture of Y-ZrO_2/Al_2O_3 composite with layers made of alumina and zirconia mixture.

increase in K_{Ic}, 50% increase in work-of-fracture and 30% increase in bending strength in comparison to the matrix and composites with barrier layers made of a mixture was observed (Table V). In the case of 50 μm thick alumina layer, a 90° crack deflection in the centre of the layer (see Fig. 12) was found. Parameter n and A (see Table V) and a plot of v-K_I (Fig. 13) confirm such a crack behaviour. As can be seen, parameter n equals 4 for composite with alumina layers in comparison to $n = 28$ for composite with the same thickness of barrier layer but made of a mixture.

Distribution of compressive stress in the barrier layers of Ce-ZrO_2/Al_2O_3 composite is similarly dependent on layer composition (Fig. 14). In an oxide mixture barrier layers compressive stress is unchangeable across the layer and independent of layer thickness. In the alumina barrier layers a difference in the compressive stress is observed. However the maximum stress at the

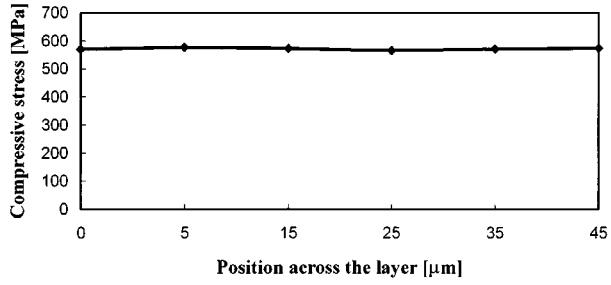

Figure 8 Distribution of compressive stress in the 45 μm thick barrier layer made of a mixture of Y-ZrO_2/Al_2O_3 composite as a function of position across the layer.

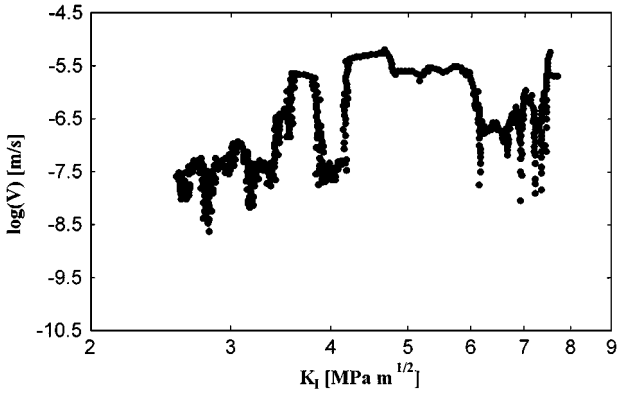

Figure 9 Crack growth rate v in Y-ZrO_2/Al_2O_3 composite with 60 μm thick alumina layers versus K_I.

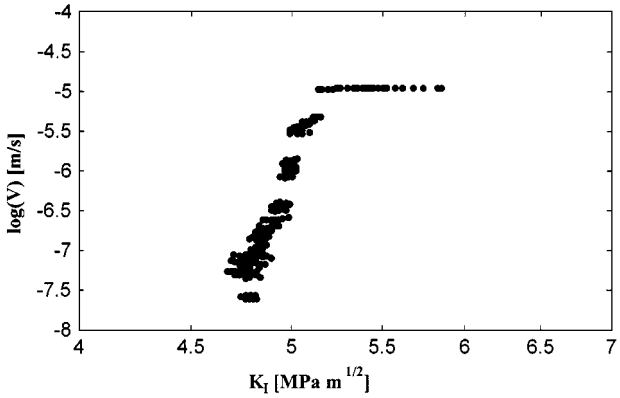

Figure 10 Crack growth rate v in Y-ZrO_2/Al_2O_3 composite with 45 μm thick barrier layers made of a mixture versus K_I.

layer boundary of Ce-ZrO_2/Al_2O_3 composite is higher than in the case of Y-ZrO_2/Al_2O_3 composite. This difference can be related to higher mismatch in the sintering shrinkage of Ce-ZrO_2 and Al_2O_3 than the same mismatch between Y-ZrO_2 and Al_2O_3 (see Table II). The width of transformation zone and the height of uplift in Ce-ZrO_2 matrix measured by Nomarski and optical interference equal 12–15 μm and 2.7μm, respectively. The same measurements made for layered Ce-ZrO_2/Al_2O_3 composites did not show any increase of these two parameters. This fact confirms the earlier thesis that the observed increase in toughness of layered composites is a result of crack deflection mechanism acting in alumina barrier layers.

4. Discussion

Ho *et al.* [14] and Oechner *et al.* [15] observations show that the stress state near the surface of the laminar composite specimen as presented in Fig. 1 seems to be more complex. The authors mentioned above found edge cracks on the surface of the thin layers that were under nominal, residual compressive stress due to the biaxial constraint of an adjacent, thicker layer with a larger α. These edge cracks appeared near the centre of the layer, propagating into the layer and running parallel to the centre line. They showed that although biaxial compressive stresses exist in the layer far from the free surface, the stress distribution near the free surface is triaxial. Specifically, the component of the triaxial stress perpendicular to the centre line of the layer is a highly localised tensile stress, which diminishes in magnitude from the surface to the interior. Ho *et al.* [14] observed that the occurrence of edge cracks was dependent on the thickness of the embedded layer and the magnitude of the residual compressive stress in the embedded layer. They found also that for a given residual stress, crack extension without any external stress takes place only when the layer thickness is greater than a critical value.

In our study the thickness of matrix and barrier layer was equal (10 to 70 μm) and edge cracks parallel to the layer were not found. But the presence of tensile stress perpendicular to the alumina layer plane with a maximum localised in the centre of the layer can be used to explain the role of compressive stress differences in the crack deflection process.

In our opinion, crack deflection in alumina barrier layers is a result of interaction of three types of stress. The first one is a residual compressive stress acting in the plane parallel to the layers found in our experiments. The second is a perpendicular tensile stress found by Ho *et al.* [14] and Oechner *et al.* [15]. Both of them are present in a laminate after cooling from fabrication temperature. And the third one is an external tensile stress applied in bending of the notched beam. As it was described, the maximum compressive stress is

TABLE V Properties of Ce-ZrO_2/Al_2O_3 composite as a function of barrier layer thickness and composition

Barrier layer composition	Mixture of Al_2O_3 and ZrO_2			Al_2O_3	Matrix of Ce-ZrO_2
Layer thickness, μm	20	50	70	50	-
Young's modulus, GPa	227.3 ± 5.0	227.3 ± 5.0	227.3 ± 5.0	286.4 ± 5.7	195.4 ± 1.0
K_{Ic}, MPa $m^{1/2}$	6.5 ± 0.3	6.9 ± 0.3	7.0 ± 0.7	11.6 ± 0.7	6.8 ± 0.1
Work-of-fracture, J/m^2	88.4 ± 5.0	87.4 ± 20.2	87.3 ± 2.1	137.9 ± 8.1	95.7 ± 4.3
Bending strength, MPa	651 ± 9	615 ± 22	633 ± 31	811 ± 19	615 ± 22
Parameter n	48.4 ± 19.3	28.1 ± 2.6	46.6 ± 4.3	4.1 ± 0.7	45.8 ± 9.8
Parameter log A	-42.9 ± 14.6	-23.6 ± 8.0	-37.5 ± 6.1	-9.2 ± 0.7	-43.2 ± 7.7

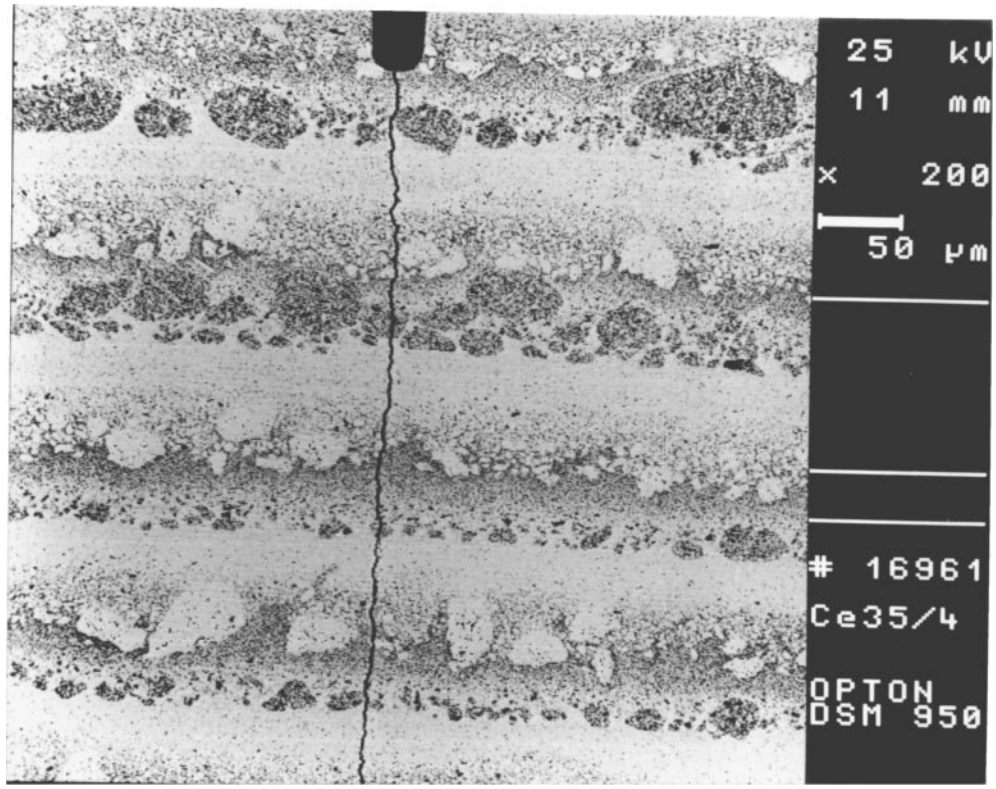

Figure 11 The crack path during fracture of Ce-ZrO_2/Al_2O_3 composites with 50 μm thick barrier layers made of a mixture.

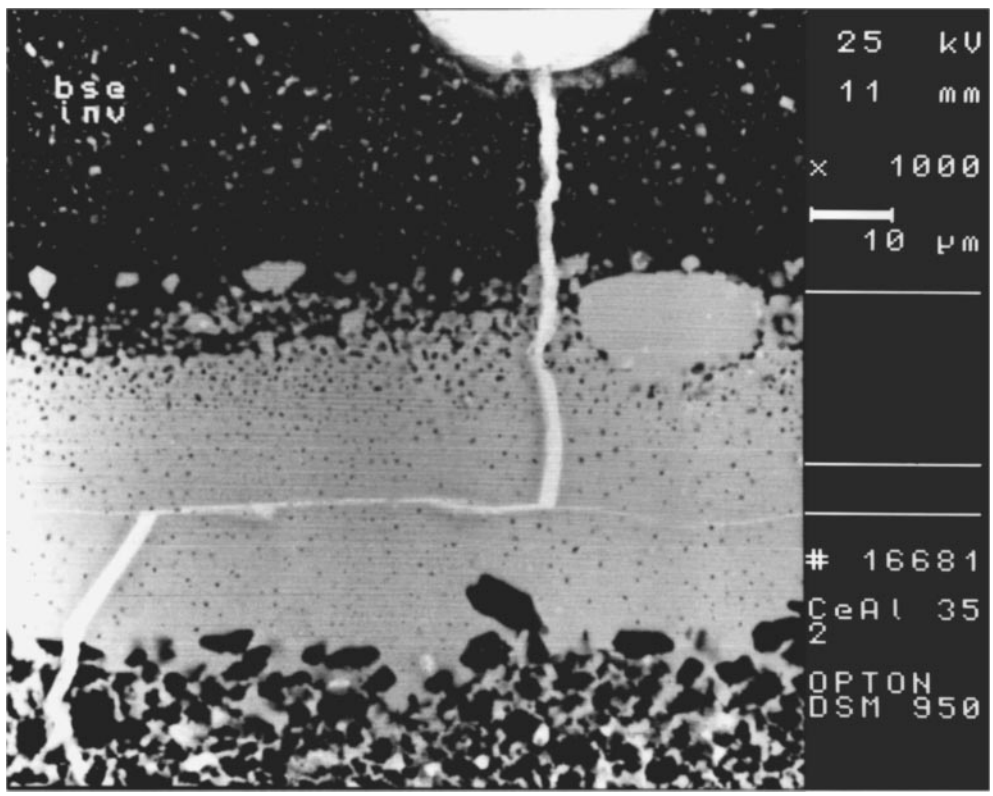

Figure 12 The crack path in alumina layer of Ce-ZrO_2/Al_2O_3 composite (inverted image).

observed at the interface and the minimum in the centre of alumina layer. After Ho *et al.* [14] and Oechner *et al.* [15], the maximum of perpendicular tensile stress exists in the centre of the barrier layer and it is also dependent on layer thickness. It means that in the centre of barrier layers with critical thickness (60 μm for Y-ZrO_2/Al_2O_3 and 50 μm for Ce-ZrO_2/Al_2O_3 composites) perpendicular tensile stress dominates. As a result, the crack deflects in the centre of the layer and propagates along the layer. When the compressive stress increases from the minimum in the centre to the maximal value at the interface, then the crack deflects back

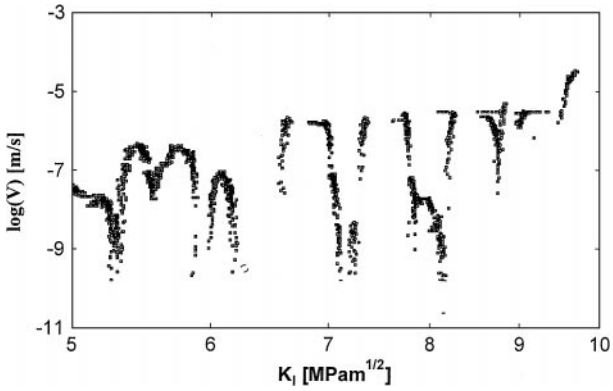

Figure 13 Crack growth rate v in Ce-ZrO_2/Al_2O_3 composite with alumina barrier layers versus K_I.

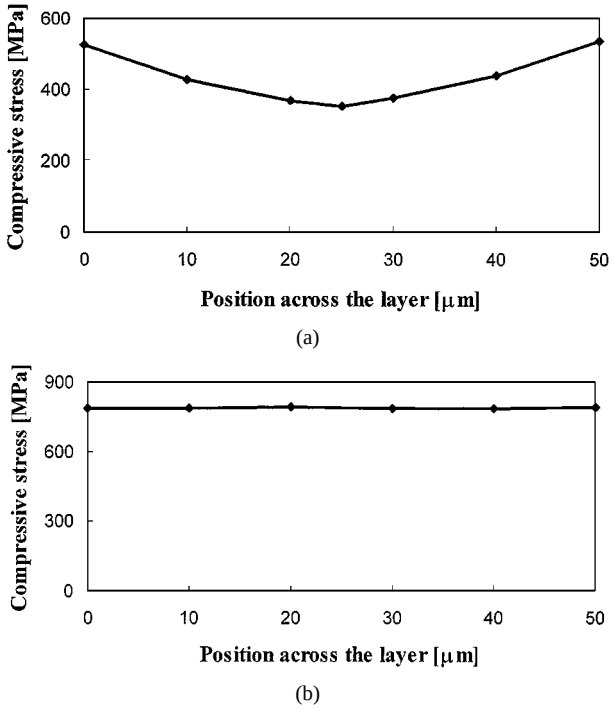

Figure 14 Distribution of compressive stress in barrier layers with thickness of 50 μm made of: a) alumina, b) an oxide mixture, of the Ce-ZrO_2/Al_2O_3 composite as a function of position across the layer.

to the original direction. In the case of the thinnest alumina layer the compressive stress across the layer becomes almost unchangeable (the stress difference is at a minimum) but when perpendicular tensile stress in the centre reaches a minimum value the crack propagates through the layer without deflection. For intermediate thickness' deflection of the crack at an angle of less than 90° is a result of combining the stresses.

5. Summary

The aim of this work was to investigate layered ceramic composites made of Y-ZrO_2 or Ce-ZrO_2 matrix layers and Al_2O_3 or Al_2O_3/ZrO_2 barrier layers. According to Marshall *et al.* [7, 8] it was expected that the presence of barrier layers would modify shape and size of the transformation zone and result in an increase of toughness of composite materials. As it happened, in our work the distinct enhancement of toughness was found only for composite with alumina barrier layers.

The controlled crack growth tests showed that the only mechanism responsible for the observed toughness increase was crack deflection. The degree of deflection was proportional to the alumina layer thickness. In the case of layer thickness lower than 10 μm the crack was undeflected during fracture. Crack deflection was not observed in the layers made of a mixture independently of layer thickness. Explanation of this phenomenon was given by the determination of residual stress distribution in barrier layers made by piezospectroscopy. As our work shows, the compressive stress at the layer boundary was independent of the alumina layer thickness. But dependence on layer thickness was found for the difference of stress between the layer boundary and the centre of the layer. A correlation between the crack deflection angle and the difference of stress was observed. Similar relations for Ce-ZrO_2/Al_2O_3 composites were noticed. Higher compressive stress at the layer boundary in this case was related to the higher mismatch in sintering shrinkage of Ce-ZrO_2 and Al_2O_3.

The only responsibility of crack deflection for enhancement of layered composite toughness was confirmed by determination of the transformation zone width by Nomarski and optical interference. The zone width for Y-ZrO_2 and Ce-ZrO_2 matrices equals 3–5 μm and 12–15 μm, respectively. However the spreading of the transformation zone in layered composites based on these two matrices was not observed. The different zone widths of Ce-ZrO_2 matrix and Ce-ZrO_2/Al_2O_3 composite compared with Y-ZrO_2 matrix and Y-ZrO_2/Al_2O_3 composite resulted in a subsequent increase in work-of-fracture found.

Acknowledgement

Supported by the Polish Committee for Scientific Research under Grant No. 7S201 04607.

References

1. R. C. GARVIE, R. H. J. HANNINK and R. T. PASCOE, *Nature* (*London*) **248** (1975) 703.
2. A. G. EVANS and R. M. CANNON, *Acta Metall.* **34**(5) (1986) 651.
3. A. G. EVANS and A. H. HEUER, *J. Amer. Ceram. Soc.* **63** (1980) 241.
4. A. H. HEUER, *ibid.* **70**(10) (1987) 689.
5. R. M. MCMEEKING and A. G. EVANS, *ibid.* **65**(5) (1982) 242.
6. J. C. LAMBROPOULOS, *ibid.* **69**(3) (1986) 218.
7. D. B. MARSHALL, F. F. LANGE and J. J. RATTO, *ibid.* **74**(12) (1991) 2979.
8. D. B. MARSHALL, *Ceram. Bull.* **71**(6) (1992) 969.
9. P. S. NICHOLSON, P. SARKAR and X. HAUNG, *J. Mater. Sci.* **28** (1993) 6274.
10. W. J. CLEGG, K. KENDALL, N. M. ALDORF, T. W. BUTTON and J. D. BIRCHALL, *Nature (London)* **347** (1990) 455.
11. D. B. MARSHALL, P. E. D. MORGAN and R. M. HOUSLEY, *J. Am. Ceram. Soc.* **80**(7) (1997) 1677.
12. M. Y. HE and J. W. HUTCHINSON, *Int. J. Solids Structures* **25**(9) (1989) 1053.
13. M. Y. HE and A. G. EVANS, *ibid.* **31**(24) (1994) 3443.
14. S. HO, C. HILLMAN, F. F. LANGE and Z. SUO, *J. Am. Ceram. Soc.* **78**(9) (1995) 1353.
15. M. OECHNER, C. HILLMAN and F. F. LANGE, *ibid.* **79**(7) (1996) 1834.

16. T. FETT and D. MUNZ, *ibid.* **75**(4) (1992) 958.
17. A. G. EVANS, in "Fracture Mechanics of Ceramics, Vol. 1: Concept, Flaws and Fractography" edited by R. C. Bradt, D. P. H. Hasselmann, F. F. Lange (Plenum Press, 1974) p. 17.
18. T. FETT, *Eng. Fract. Mech.* **40** (1992) 683.
19. J. HE and D. R. CLARKE, *J. Amer. Ceram. Soc.* **78**(5) (1995) 1347.
20. N. L. HARRISON and W. J. HARRISON, *J. Adhes.*, **3** (1972) 195.
21. H. KIRCHNER, J. CONVAY and A. E. SEGALL, *J. Am. Ceram. Soc.* **70**(2) (1987) 104.

Received 5 May
and accepted 22 December 1999